Acoustic emission for on-line monitoring of damage in various application fields

Martine Wevers, Gert Van Dijck, Wendy Desadeleer, Mark Winkelmans° and Koen Van Den Abeele*
Katholieke Universiteit Leuven
Department of Materials Engineering, Kasteelpark Arenberg 44, B-3001 Leuven
*Katholieke Universiteit Leuven, Afdeling Kortrijk
Subfaculty of Sciences, Sabbelaan 53, B-8500 Kortrijk
°BASF AG, Carl-Bosch-Straβe 38, D-67056 Ludwigshafen

ABSTRACT

Structural damage in materials is a “top priority” to be investigated by material scientists all over the world. The future or limit of a material to be used in structural applications depends upon it, as safety and environmental protection are important issues in national policies.
The acoustic emission technique offers the possibility to listen to the damage process when and where it occurs. This paper focuses on a number of cases investigated at the department MTM using acoustic emission to analyse damage in various application fields. The tools handled to interpret the AE signals, the relation between AE and the residual properties and the additional understanding of a particular material behaviour will be outlined. The fatigue damage of CFRP, the curing of concrete and the corrosion of carbon steel and stainless steel will be handled as case studies.

Introduction

The acoustic emission technique is a “passive” method which detects the elastic energy released when microstructural changes in a material or a process take place. The AE sensors, mostly PZT transducers, resonant or broadband are used to pick up the elastic stress waves from the material and convert them into an electrical signal. This electrical signal is further processed by filters, amplifiers and a signal processing unit (PC). Depending on the application the correct frequency bandwidth has to be chosen to ensure the best sensitivity of the detection system for the phenomena to be measured. The sampling rate also depends upon the latter. The further tuning of the signal-to-noise ratio (filters/amplifiers) can be done to optimise the monitoring conditions. For the analysis of the AE data it can be of help that with the AE signal also a recording is done of the time of loading or the loading itself (mechanical or thermal). From the AE signal itself the following parameters or AE characteristics are recorded: amplitude, duration, ringdown counts, rise time, energy, slope, frequency, modal content of the AE signal, AR (auto regressive) and wavelet parameters.

Case study one: Fatigue damage monitoring of carbon fibre reinforced epoxy laminates with AE

Tension-tension fatigue tests have been performed on quasi-isotropic $(0°, +45°, 90°, -45°)_s$ carbon-epoxy laminates at different R-ratios. The typical damage development curve of this type of laminate lay-up is depicted in figure 1. From this curve it is said that the first increase in damage is caused by matrix cracking (stage I). Matrix cracking is then

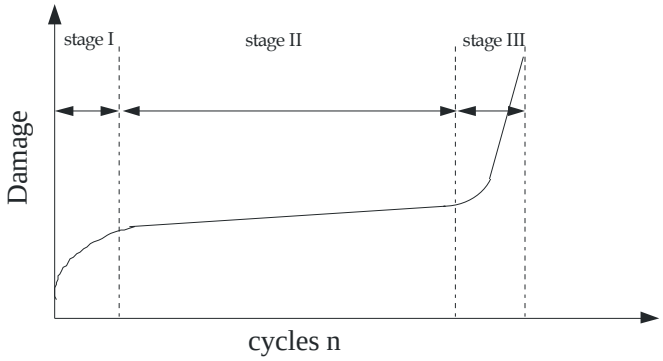

Figure 1: Typical damage development curve for quasi-isotropic composites

followed by a steady state growth of delaminations in stage II and in the final stage III fibres are broken leading to the final failure of the composite.
In figure 2, where the total counts of the "filtered" AE are depicted as a function of fatigue cycles of a fatigue test run at S_{max} = 70% of the UTS and R=0,3 at a frequency of 3 Hz, the shape of figure 1 can be identified as well. Elaborated studies of the damage development, using replica's, X-ray radiography with penetrants and ultrasonic C-scans identified matrix cracking in stage I, more matrix cracking and delamination in stage II and fibre failures in stage III. The filter consisted of only counting the AE counts in the upper 20% of the sinusoidal loading cycle, which hereby excludes the AE signals generated by crack closure.

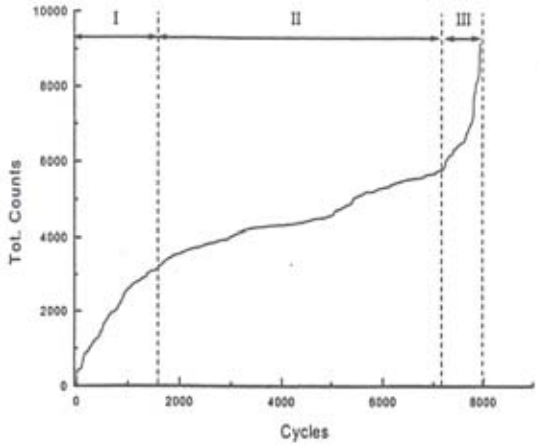

Figure 2: Cumulative counts versus cycles for filtered AE S_{max} = 70% UTS, R = 0.3

Taking this evidence into account an attempt was made to model the fatigue behaviour of the composite using the AE counts as an input.
For stage I it was obtained that: $n_I = n_{ini} + n_f$, where n_{ini} is the cumulative counts during quasi-static loading and n_f the cumulative counts during fatigue loading where $dn/dN = A_1 \sigma^{2c}_{max} / cn^{c-1}$, so $n_I = (A_1 \sigma^{2c}_{max} N + n^c_{ini})^{1/c}$ and A_1 and c constants to be defined as a function of the applied stresses.
For stage II the variation of the cumulative counts with fatigue cycles $dn_{II}/dN = A_2 (\Delta\sigma/\sigma_u)^{\gamma}$ with A_2 and γ the constants to be defined by plotting dn_{II}/dN as a function of $\Delta\sigma/\sigma_u$, being the fatigue stress amplitude divided by the tensile strength of the composite. It was found that for this composite A_2=32,3 and γ=10,2.
For stage III a problem arises when the final damage development is not located in between the monitored region as was the case for a 'certain' number of fatigue tests. [1]

The results presented indicate clear that the damage development in a composite can be monitored with the acoustic emission technique whenever the whole critical area is being monitored and the modelling of non-linear behaviour (D) can be done based on AE data from the critical region when the modelling parameter is related to physical damage. Once the material behaviour is characterized by such curves, monitoring the slope of the AE cumulative counts with the number of fatigue cycles can identify the damage stage the QI composite material is in.

AE system used: Vallen AMS-3 AE System, DECI 375M AE-sensors

Case study two: Cure monitoring of concrete with AE

Another application of the use of AE is the on-line monitoring of curing processes in freshly poured concrete. The ultimate goal for monitoring concrete during its setting is to predict the long-term behaviour of concrete and to interpret the dependence of this behaviour on the initial composition and initial drying conditions of the concrete. [2]
Preliminary monitoring tests were performed in the laboratory, using a curing cell (figure 3) of 200×150×100 mm³, instrumented with 2 AE sensors, a temperature sensor (T) and 2 ultrasonic transducers (U). Concrete of the following composition was used: 1.88 kg sand, 3.57 kg aggregates, 1.35 kg CEM I 42.5R, 0.45 l water and 13.5 cc Rheolmild. The curing cell was placed in an environmental chamber (Heraeus-Vötsch Climate Cabinet VLK 04/150) to isolate it from variations in outside temperature and humidity. However, the climate conditions were not controlled, allowing variations in temperature inside the concrete sample.

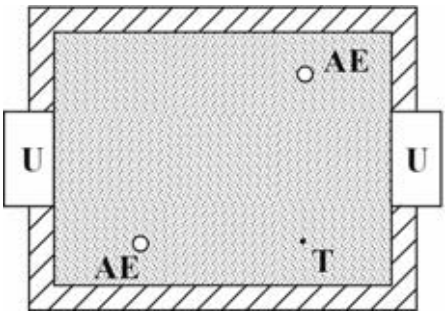

Figure 3: Top view of the curing cell instrumented with 2 AE sensors, a temperature sensor (T) and 2 ultrasonic transducers (U)

The curing process during the first 72 hours was monitored, measuring the cumulative counts of the AE events due to cracking, which is caused by the setting of the material during hardening. Apart from real curing related AE events, the received AE signals (figure 4a: original data) also consist of mechanical noise and EMI signals. The high frequency signals (figure 4b) can easily be distinguished from the low frequency AE events (figure 4c) and were filtered out by applying a low pass filter on both channels, generating the “filtered” AE data (figure 4a).

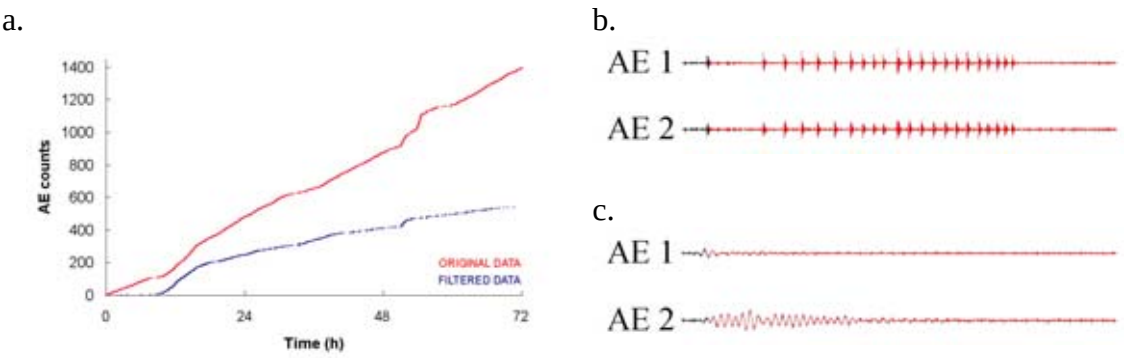

Figure 4: a. Cumulative counts of the original AE data and the "filtered" events
b. Example of a high frequency signal (spurious AE event)
c. Example of a low frequency AE event

Simultaneously with the AE measurements, the temperature inside the concrete cell was registered and the evolution in the compressional wave velocity during hardening was derived from the time of flight of an ultrasonic compressional pulse which was sent through the sample every 10 minutes. Figure 5a illustrates the correlation between the cumulative counts of the filtered AE events and the temperature variations inside the concrete sample. A first increase in the AE events after 9 hours corresponds with an increased inside temperature. Figure 5b shows that this increase in AE events occurs when the compressional wave velocity is almost stabilized. The first, and most important, increase in temperature is caused by an acceleration of the –exothermal– hydratation reactions which reach a peak value after 11 hours, when the hydratation reaction is at its maximum efficiency. This acceleration is also noticed in the evolution of the compressional wave velocity in time, indicating a stage of increased hardening. When the hydratation reaction is at its maximum efficiency, the concrete sample is almost completely cured, and the velocity remains at a more stable level after 11 hours. The first increase in the cumulative counts of the filtered AE events can thus be explained by intensification in microcrack generation at the final phase of the main concrete setting and shrinkage process (<20 hours). At later stages, microcracking is caused by further curing and by temperature variations due to day/night cycles, which are also detected in the cumulative counts of the filtered AE events.

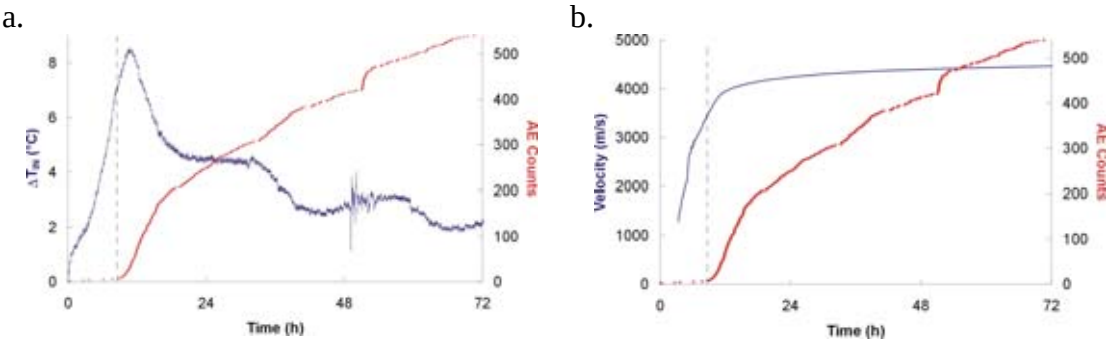

Figure 5: Cumulative counts of filtered AE events in comparison with (a) the variations in inside temperature and (b) the evolution of the ultrasonic wave velocity.

AE system used: Fracture Wave Detector, Digital Wave Co., VS375-M 340 AE-sensors

Case study 3: Corrosion monitoring of carbon steel and stainless steel by means of advanced data analysis and AI techniques on AE-signals

A lot of failures in chemical process installations are due to corrosion processes. Literature [3] mentions that annually 3 to 5 % of the G.N.P. in industrialized countries is lost directly or indirectly due to corrosion processes. Conventional non-destructive testing techniques such as visual inspection, ultrasonic testing, penetrating testing, magnetic testing and radiographic testing are most frequently used to evaluate corrosion in chemical installations [4]. All these techniques are typically applied when the installation is taken out of service during periodic inspections. These techniques are insufficient when a considerable amount of corrosion has taken place between 2 periodic inspections.
A continuous corrosion monitoring system obtrudes. Acoustic emission offers the possibility to listen continuously to the materials while damage is developing. Typical acoustic emission signals could offer operators the alarm to inspect installations while damage is occurring. By immediate response to the occurring damage one can avoid that aggressive chemicals are liberated such that risk for people and environment is minimized.
This case study focuses on identifying 3 most important corrosion processes for chemical industry by means of the acoustic emission technique: uniform corrosion, pitting and stress corrosion cracking (SCC). Corrosion processes were induced on carbon steel (DIN 1.0038) and stainless steel (DIN 1.4541). The number of selected signals for each corrosion process is:

- 102 pitting events (brackish water + $FeCl_3$ 1% at 60 °C)
- 43 SCC signals in stainless steel ($CaCl_2$ 40% at 80 °C)
- 42 SCC signals in carbon steel ($Ca(NO_3)_2$ 60% at boiling point)
- 81 uniform corrosion signals in carbon steel (H_3PO_4 10% at room temperature)

The generated acoustic signals in the different corrosion processes are highly dependent on the geometry of the material. In order to guarantee reproducible results and to facilitate up scaling from laboratory to chemical plant installations the research focused on a fixed geometry of a reference probe to monitor the signals. The corrosion damage on the probe needs to be representative for the damage on the chemical installation. This implies that the material of the probe underwent the same treatment as the material of the installation. Critical stress locations in the installations need to be identified, the same stresses need to be applied to the reference probe. The experimental set-up has been published in [5,6].
Two reference probes are partially submerged in the corrosive environment. When transient signals are detected simultaneously these are likely due to system influences (flow of the chemical or pressurized air) or due to environmental influences (electromagnetic interference, mechanical vibrations, …). The third probe is placed in a non-corrosive environment. Simultaneous transients on all 3 probes are due to environmental influences (electromagnetic interference, mechanical vibrations, …).
Transients that could be related to system or environmental influences are not retained within the data analysis.

Data analysis

Different steps were undertaken to achieve an automatic classification of the different corrosion processes. First different filtering (denoising) techniques were tried out to increase the signal-to-noise ratio.

The filtering techniques applied are: spectral subtraction [7], NLMS (Normalized Least Mean Squares, adaptive filtering) [8], signal subspace filtering and an enhanced form of signal subspace filtering [9].
Second the denoised time signals are transformed for feature extraction. The transformations applied are: FFT (Fast Fourier Transform), AR-model (Auto Regressive model) [10] and a Wavelet transform [11]. The FFT allows characterizing the time signals in frequency domain, the AR-model in time domain and the Wavelet transform in frequency-time domain. The best results in classification were obtained in frequency domain (FFT).
512 samples were selected in each time series and the FFT was applied. This results in 512 samples in the frequency domain. Only half of the spectrum is retained because real time series result in a symmetric spectrum, the second half contains no additional information.
Third the information in the frequency domain, 256 frequencies with corresponding amplitudes, is compressed in a few parameters. The Principal Component Analysis (PCA) [12] was applied to extract important parameters from the frequency domain. PCA finds projections of the data such that variance in data is maximal after each projection, with the constraint that projection axes are orthogonal.
In a fourth step the visualization of the data is done by estimating the probability density function (PDF) of the data in 2D space, after projecting the frequency data on the 2 most important principal axes (vectors) of the PCA. If different corrosion processes fall apart in different clusters, a classification machine should be successful in separating different corrosion processes. Different clusters can be detected by means of the maxima in the PDF. This allows determining qualitatively the quality of the transform on the time series, after PCA, independent of the chosen classification procedure. The density was estimated by means of an unsupervised neural network: Kohonen self-organizing map [12], see figure 6 and figure 7.

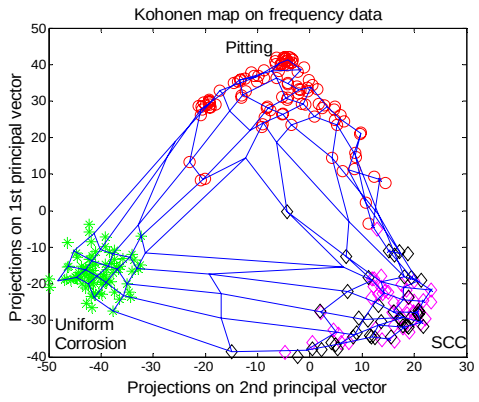

Figure 6: Visualization of data.
Every time series is reduced to 2 parameters (by means of PCA) for which the values are put on the X- and Y-axis. The grid overlaying the data is the Kohonen self-organizing map. The crossings of the grid are the neurons of the neural net. The neurons are distributed over the data in order to represent the density of the data.

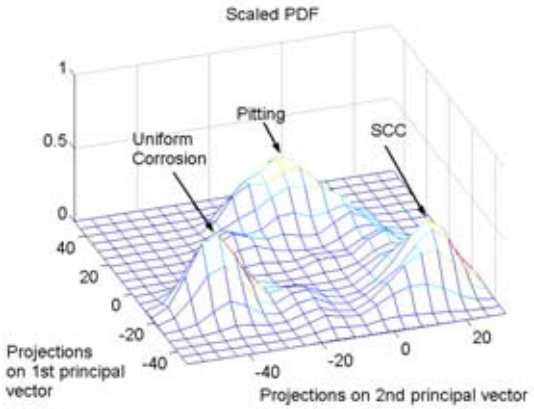

Figure 7: Probability density estimate.
Figure 7 is derived from figure 6 by putting Gaussian kernels on the grid crossings over the neural net. Maxima in the density estimate represent different clusters.
Every cluster corresponds with a different corrosion class. The density estimate allows describing the transform (and PCA) qualitatively independent of the classification procedure.

The kernel widths of the Gaussian kernels, which are centred on the neurons, are tuned automatically by using the least-squares cross-validation method [13]. Only for the FFT different corrosion classes resulted in separate clusters, see figure 7. The wavelet transform merged all data in 1 cluster. The AR-model merged pitting and SCC in 1 cluster and resulted in a separate cluster for uniform corrosion.
From this it can be concluded qualitatively that the FFT is the most appropriate transform to distinguish between different corrosion classes.

For quantitative assessment of separability, the least squares support vector machine (LS-SVM) [14] classification procedure is used.
The function to be minimized in LS-SVM's is defined by:

$$\min_{\mathbf{w},b,e} Jp(\mathbf{w},e) = \frac{1}{2}\mathbf{w}^T.\mathbf{w} + \gamma\frac{1}{2}\sum_{k=1}^{N} e_k^2 \qquad (1)$$

such that $y_k.\left(\mathbf{w}^T.\varphi(\mathbf{c}_k)+b\right) = 1-e_k,\ k=1,...,N$ (2)

For a binary classification problem the classifier y(c) takes the form:

$$y(\mathbf{c}) = sign\left(\mathbf{w}^T.\varphi(\mathbf{c})+b\right) \qquad (3)$$

The **w** in (1) is related to the margin between different classes in the feature space.
Minimizing $\frac{1}{2}\mathbf{w}^T.\mathbf{w}$ results in maximizing the margin, see figure 8.

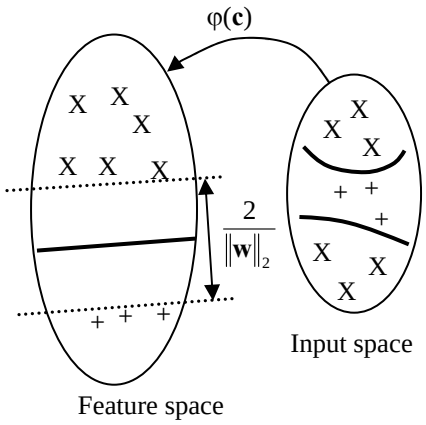

Figure 8: X: data points of a 1st class. +: data points of a 2nd class. In the feature space a linear decision boundary is computed. $\frac{2}{\|\mathbf{w}\|_2}$ is the margin between the 2 different classes.

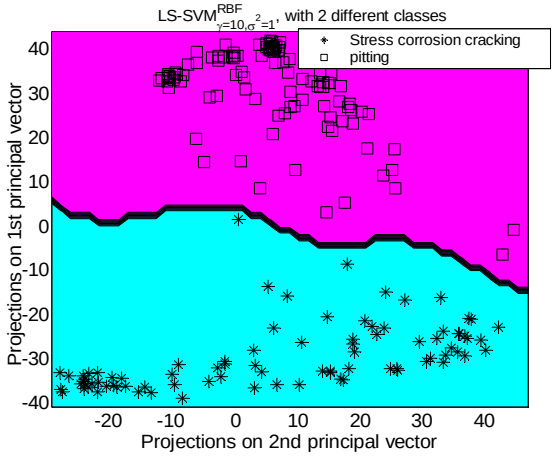

Figure 9: Decision boundary computed by the LS-SVM. In this case the LS-SVM was able to separate all SCC signals (asterisks) from the pitting signals (squares). All symbols are time series, with information compressed in 2 parameters after FFT. $\mathbf{C_k}$'s are represented by the data points.

In SVM's the input space is defined by the data points: the $\mathbf{c_k}$. The feature space is defined by the $\varphi(\mathbf{c_k})$, see figure 8. The φ-mapping is a transformation to a higher dimensional feature space. In this higher dimensional feature space a linear separation is made between the different classes.
The second term in (1) tries to minimize the classification error. When γ is large less training examples will be misclassified, but this might result in overfitting. The margin will allow for generalization. y_k in (2) is the class label, for a first class this is chosen +1 for a second class –1. The 1 on the right hand side in (2) is a target value, in case of overlapping distributions between classes some error e_k is allowed on the target value.

The constrained optimization problem (1)-(2) can be solved easily by defining the Lagrangian of the problem:

$$L(\mathbf{w},b,e;\boldsymbol{\alpha}) = J_p(\mathbf{w},e) - \sum_{k=1}^{N} \alpha_k \left\{ y_k \left[\mathbf{w}^T . \varphi(\mathbf{c}_k) + b \right] - 1 + e_k \right\} \quad (4)$$

In the general case the φ-mapping can become infinite dimensional and a so-called dual problem is solved. The dual problem is defined by the search for the optimal Lagrangian multipliers: α_1, α_2… α_N of the constrained optimization problem. Solving the primal problem corresponds to searching for the optimal **w**. It can be shown that optimal α is found by solving a set of linear equations. The advantage of the dual problem is to circumvent the problem of the possible infinite φ-mapping. The classifier in the dual space takes the form:

$$y(\mathbf{c}) = sign\left[\sum_{k=1}^{N} \alpha_k . y_k . K(\mathbf{c}, \mathbf{c}_k) + b \right] \quad (5)$$

with $K(\mathbf{c},\mathbf{c_k}) = \varphi(\mathbf{c})^T.\varphi(\mathbf{c_k})$ (6)

By solving the dual problem all φ disappear and are replaced by kernels of the form in (6). This is known as the kernel trick. In practice different kernels can be chosen: linear, polynomial, radial basis function (RBF), … . The RBF kernel takes the form:

$$K(\mathbf{c}, \mathbf{c}_k) = \exp\left(\frac{-\left\| \mathbf{c} - \mathbf{c}_k \right\|_2^2}{\sigma^2} \right) \quad (7)$$

For the classification problem both the linear kernel and the RBF-kernel were tried out, results were slightly better with the RBF-kernel. Classification results were always better for the data after the FFT compared to the wavelet transform and the AR-model. This could be expected while the FFT was the only transform that resulted in separate clusters for each corrosion class. The classification problem was solved by solving 2 binary classification problems using 10 fold cross-validation. In a first step uniform corrosion was separated from the other 2 classes (considered as 1 class). This could be achieved practically without error. In a second step pitting was separated from SCC. This could be achieved with about *1% classification error* on average. Best results were obtained when using the spectral subtraction filtering technique. Figure 9 shows an example of the decision boundary computed by the LS-SVM.

All programs were partially developed in the C-programming language (Kohonen self-organizing map) and MATLAB. The LS-SVM was available as a software tool, developed at the Department of Electrical Engineering (ESAT), at the Katholieke Universiteit, Leuven.

AE system used: Fracture Wave Detector, Digital Wave Co., B1025 Digital Wave AE-sensors

Conclusions

Modelling the material behaviour based on NDT data is gaining more interest as the confidence in the techniques increases, as the relation with physical damage is proven. The on-line monitoring of fatigue in CFRP laminates and of the curing of concrete with AE results in cumulative AE counts which after filtering offer the input data to model the damage behaviour of the material. The AE technique offers parameters linked with physical damage to do the modelling with.

More sophisticated signal processing of the AE signals is also presented in order to extract features from the time signals; subsequently these features are used as input for a classification machine in order to identify different corrosion processes.

Case study 1: Research funded by the EC human capital and mobility fellowship
Case study 2: Research funded by the FWO, Flemish Fund for Scientific Research
Case study 3: Research funded by a Ph.D. grant of the Institute for the Promotion of Innovation through Science and Technology in Flanders (IWT-Vlaanderen).

1. Tsamtsakis, D. and Wevers, M., “Acoustic emission to model the fatigue behaviour of quasi-isotropic carbon-epoxy laminate composites”, INSIGHT – Non-Destructive Testing and Condition Monitoring (The Journal of The British Institute of Non-Destructive Testing), vol. 41, no. 8, August 1999, pp. 513-513.
2. Lacouture, J.-C., “Modélisation de l'évolution des coefficients mécaniques du béton pendant la prise. Liaison avec les mesures ultrasonores linéaires et non linéaires” Thèse, UFR De Physique, 2002, Université Paris 7 – Denis Diderot, 201p.
3. National Bureau of Standard/US Department of Commerce, “Economic effects of metallic corrosion in the United States”, NBS, Special Publication 511-1, Washington DC, 1975
4. Rudlin J.R., “Review of existing and possible techniques for corrosion under insulation and wall thickness measurement in steel pressure containments”, Insight vol. 39, no. 6, 1997, pp. 413-416.
5. Winkelmans, M. and Wevers, M., “Non-destructive testing for corrosion monitoring in chemical plants, Journal of Acoustic Emission”, vol. 20, 2002, pp. 206-217 (CD-ROM).
6. Winkelmans M., Ph.D., “Fusion of non-destructive inspection techniques for corrosion monitoring in chemical process installations”, Katholieke Universiteit Leuven, ISBN 90-5682-484-8, UDC 620.179:620.193.4, University of Leuven, 2004.
7. Boll, S.F., “Suppression of acoustic noise in speech using spectral subtraction”, IEEE Transactions on Acoustics, Speech and Signal Processing, vol. ASSP-27, no. 2, April 1979.
8. Moonen M., Proudler I., “Introduction to adaptive signal processing”.
9. Hu Y., Loizou C., “A subspace approach for enhancing speech corrupted by colored noise”, IEEE Signal Processing Letters, vol. 9, no. 7, July 2002.
10. Chatfield C., “The analysis of time series”, Chapman & Hall, 1987.
11. Daubechies I., “Ten lectures on wavelets”, Society for Industrial and Applied Mathematics, Philadelphia, Pennsylvania 1999.
12. Ham F.M., Kostanic I., “Principles of neurocomputing for science & engineering”, McGraw-Hill Higher Education, 2001.
13. Silverman B.W., “Density estimation for statistics and data analysis”, Chapman & Hall, p. 106-107, 1992.
14. Suykens J.A.K., Van Gestel T., De Brabanter J., De Moor J., Vandewalle J., “Least squares support vector machines”, World Scientific Pub. Co., Singapore, 2002.